In-Situ Detection of Inclusions in Liquid Steel

Xiaodong Wang, Roderick I.L.Guthrie* and Mihaiela Isac
*Corresponding author: Director, McGill Metals Processing Centre, 3610 University Street, M.H.Wong Building, Room 2M040, Montreal, H3A 2B2, Canada. rod@mmpc.mcgill.ca

Abstract: A numerical multiphase flow model is proposed to predict the behaviour and motion of entrained inclusions in liquid steel, as they enter the orifice of a LiMCA (Liquid Metal Cleanliness Analyzer) sensor for assuring steel quality. The method of measurement is based on the electric sensing zone (ESZ) technique. The liquid metal flow field within the ESZ is obtained by solving the Navier-Stokes equations taking into account the presence of a self-induced electromagnetic field. When an entrained non-conducting inclusion passes through the orifice of the probe, in the presence of a direct current, the change in the electrical resistance of the ESZ due to its presence in the ESZ can register a resistive pulse. Such signals, in turn, can be used to detect the numbers and sizes of entrained inclusions. The trajectories of these entrained inclusions have been modeled using a momentum equation by solving Comsol ODE, External forces acting on the particles include those for standard drag (Stokes), added mass, fluid acceleration, buoyancy and, most significantly, electromagnetic. The boundary effects on Stokes drag are also taken into account. Predicted voltage pulse signals are compared with experimental values derived from some water-based LiMCA experiments

Keywords: discrimination of inclusions, multiphase flow, liquid steel, particle motion, trajectory, electromagnetic force

1. Introduction

LiMCA (Liquid Metal Cleanliness Analyzer) is a technique for the in-situ, online detection of inclusions in liquid metals. Developed at McGill University in the early eighties, it has seen rapid development in the past two decades [1-4]. After several key technical problems had been solved, it was first supplied commercially to the aluminum industry in 1985. More recently, a version of the system has been offered to the steelmaking industry. Concerning the LiMCA system for molten steel, the much higher temperatures (1600 °C vs. 700°C), and much lower electrical conductivity vs. liquid aluminum (1/5), meant that the ESZ had to be redesigned, and the new set of operating parameters optimized. The fundamental aspects of the transient voltage pulses associated with the passage of inclusions in molten steel passing through the ESZ still need to be clarified and justified. In order to help realize these objectives and to validate numerical predictions, a laboratory-scale water-based LiMCA experimental modeling system has also been developed [3, 8]. The advantage of a water-based model of the high temperature ESZ system, is the relative ease of collecting good experimental data.

2. Governing Equations:

The present paper deals with the following governing Equations:

2.1 The continuity and incompressible Navier-Stokes equations:

$$\nabla \cdot \mathbf{u} = 0 \tag{1}$$

$$\rho_f \mathbf{u} \cdot \nabla \mathbf{u} = -\nabla p + \mu_f \nabla^2 \mathbf{u} + \mathbf{F}_{em} \tag{2}$$

where

$\mathbf{u}(u, v)$ velocity vector of liquid steel;

p pressure;

ρ_f, μ_f density and viscosity of liquid steel;

$\mathbf{F}_{em}$ Lorentz force density exerting on the liquid steel.

The liquid steel flow within the ESZ is assumed to be in steady, laminar flow due to its low Reynolds number (if the diameter of the throat of the orifice is taken as the typical length scale, D=500μm characterizing the fluid flow, and the typical velocity is 1m/s, then Re=560).

2.2 Electromagnetic Force Equation:

The quasi-static electromagnetic sub-module within the AC/DC module of Comsol was used

to compute the electromagnetic force generated by DC current passed through the liquid steel within the ESZ. The cylindrical coordinate system (r, z, θ) was used for liquid within the ESZ.

The Lorentz electromagnetic force is defined as:

$$\mathbf{F}_{em} = \mathbf{J} \times \mathbf{B} \tag{3}$$

where
$\mathbf{J} = -\sigma_e \cdot \nabla\varphi$ (Ohm's law). Here, **J** is the electric current density, σ_e is the electrical conductivity, which, for steel, is $7.194 \times 10^5\ \Omega^{-1} m^{-1}$, and $\nabla\varphi$ is the electric potential. $\mathbf{B} = \nabla \times \mathbf{A}$ is the self-induced magnetic field within the ESZ, where **A** is the magnetic vector potential. The electric potential can be solved through the Laplace equation:

$$\frac{1}{r}\frac{\partial}{\partial r}\left(r\frac{\partial\varphi}{\partial r}\right) + \frac{\partial^2\varphi}{\partial z^2} = 0 \tag{4}$$

The self-induced magnetic field is derived from Ampere's law:

$$\oint_C \frac{B}{\mu_0} \cdot dl = \int_S J \cdot dA_S = I \tag{5}$$

where
$\mu_0 \left(= 4\pi \times 10^{-7}\ H/m\right)$ is the magnetic permeability in free space; I is the input electric current.

2.3 The equation of motion for entrained inclusions:

To predict the trajectories of a rigid, spherical non-conducting inclusion, the momentum equation can be expressed according to equation 6 (see reference [4]);

$$\begin{aligned}\frac{\pi}{6}d^3\rho_p\frac{d\mathbf{u}_p}{dt} &= \frac{\pi}{8}d^2C_D\rho_f\left|\mathbf{u}_\mathrm{f}-\mathbf{u}_\mathrm{p}\right|\left(\mathbf{u}_\mathrm{f}-\mathbf{u}_\mathrm{p}\right)\\ &+\frac{\pi}{6}d^3\rho_f\frac{D\mathbf{u}}{dt}\\ &+\frac{\pi}{6}d^3C_M\rho_f\left(\frac{D\mathbf{u}_\mathrm{f}}{Dt}-\frac{d\mathbf{u}_p}{dt}\right)\\ &+\frac{3}{2}d^2\left(\pi\mu_f\rho_f\right)^{1/2}\int_0^t\frac{d(\mathbf{u}_\mathrm{f}-\mathbf{u}_\mathrm{p})/ds}{(t-s)^{1/2}}ds\\ &+\frac{\pi}{6}d^3\left(\rho_f-\rho_p\right)\mathbf{g}\\ &-\frac{3\pi}{8}d^3\mathbf{F}_{\mathrm{em}}.\end{aligned} \tag{6}$$

with the initial condition:

$$u_p(t=0) = u_f(t=0). \tag{7}$$

In Eq.(6), the term on the left-hand side represents the force required to accelerate the inclusion. The first term on the right-hand side models viscous resistance according to Stokes's law. C_D is the drag coefficient which can be expressed as $C_D = \frac{24}{\mathrm{Re}_p}\left(1 + 0.15\,\mathrm{Re}_p^{0.687}\right)$ based on the Reynolds number of the inclusion:

$$\mathrm{Re}_p = \left(\rho_f d\left|u - u_p\right| / \mu\right) \tag{8}$$

The second term is due to the pressure gradient resulting from the acceleration of the liquid steel. Note that the derivative of fluid velocity with respect to time is in an Eulerian form: $D\mathbf{u}_\mathbf{f}/Dt = d\mathbf{u}_\mathbf{f}/dt + \mathbf{u}_\mathbf{f} \cdot \nabla\mathbf{u}_\mathbf{f}$. The first term on the right-hand side is zero.

The third term in equation (6) is the force required to accelerate the apparent mass of the inclusion relative to the ambient liquid steel.

The fourth is Basset history force. In present study, the inertial effect is much higher than that of the drag. In such circumstances, history force can be omitted.

The fifth term is the buoyancy force. Again, under the set of operating condition applying for LiMCA, the buoyancy term has a negligible influence on the motion of the inclusion.

The sixth term is the electromagnetic body force on the inclusions. $\mathbf{F}_{em}$ denotes the

electromagnetic force density exerting on the liquid steel at the position of the inclusion.

The presence of a solid orifice wall in the vicinity of a moving particle will affect the drag force. In such shaped orifice, the enclosure effect on drag force can be considered as the influence of a varying cross-section (parabolic asymptote) cylindrical body. Fayon proposed a method to introduce a multiplier in the axial component of the drag force [5]:

$$K_{wall} = 1/(1 - 2.0144k + 2.0888k^3), \quad (9)$$

where
$k = d/d_{cs}$, the diameter ratio of the inclusion d and the varying cross-section of the orifice d_{cs}. On the other hand, the influence of the orifice wall in the radial direction on the drag force is described in reference [6].

$$C_d = \frac{32}{\mathrm{Re}} f \quad (10)$$

where:
f is a function in term of the ratio of the distances from the particle geometry centre to the orifice wall. A tabulated correction factor for the axial drag force on a particle moving perpendicular to a plane wall was used [6].

2.4 Inclusions register transient electric resistance pulses when passing the ESZ:

The electric resistance of the ESZ without an inclusion inside is given by Ohm's law [7]:

$$R = \rho_e \int \frac{dz}{A(z)} \quad (11)$$

where
ρ_e electrical resistivity of the liquid steel;
$A(z)$ the average surface area of the equi-electric potential over an element distance dz.

The computation of the resistance pulse was obtained by a numerical integration method. When a non-conducting spherical inclusion is entrained into the ESZ, the resistive pulse generated is obtained by:

$$\Delta R = \rho_e \sum_{z_p - d/2}^{z_p + d/2} \frac{\Delta z \cdot S_{ep\_i}}{S_{ep\_f}\left(S_{ep\_f} - S_{ep\_i}\right)} \quad (12)$$

where
S_{ep_f} and S_{ep_i} are the occupying surface areas on each electric potential contour (equi-potential) of the liquid steel and the inclusion, respectively. Here, we neglect the influence of electric potential redistribution within the inclusion due to its small size compared with the liquid domain. $\Delta z = d/100$, was selected as the length step in the *z*-direction. The integration form of Eq. (12) is the fundamental formula for the *in-situ* detection of inclusions used in the LiMCA system. The curvature areas of equi-potential are computed by exporting the contour potential data from the Comsol to the Excel of Microsoft office, and these are then are plotted with a Matlab program.

3. Numerical method:

This multiphase flow problem, involving entrained inclusions within the liquid steel is model using Comsol Multiphysics. The steady liquid flow through the ESZ is first computed. Meanwhile, the Lorentz electromagnetic force, set as the source term in the Navier-Stokes Equations, is solved. Then, the particle tracing function in the postprocessing is used to predict the motion of the particle using a Lagrangian approach. The equation is based on the Newton's second law and the momentum equation is solved with a Comsol internal ODE. A specifically particular model was developed instead of the default model of Khan and Richardson.. The boundary effect is related to the distance between the inclusion and the wall, which can be readily computed by defining a boundary distance variable. Note that the quadratic elements are used to fit the parabolic orifice computing domain, and precisely compute the curvature areas of the equi-electric potential.

4. Results:

4.1 The electromagnetic force distribution:

The electromagnetic force field is self-created by the input of a direct current passing

through the electric sensing zone (ESZ) from the inner anode inside the tube, to an outer cathode. A typical input electric current I=15A for the liquid steel LiMCA is used in the present study. Note that in such cases of lower magnetic Reynolds number, the electromagnetic field is little influenced by the velocity of the liquid steel flow. As seen in Fig 1, the vector potential ***A*** has a similar distribution to the current density, ***J***. Hence, according to Ampere's law, the azimuthal magnetic flux density B_θ plays a dominant role. B_θ is at its highest value near the wall and drops off to virtually zero at the central-axis of symmetry.

As can be seen in Fig 2, representing the upper left-half of the ESZ orifice, the predicted equi-potential contours along the central cross section of the orifice are the highest and then drop gradually towards zero near the entrance to the ESZ. These contours are always perpendicular to both the z-axis of symmetry and to the parabolic orifice wall. The total voltage difference across the orifice is about 0.05V when I=15A. The electro-magnetic body force on the liquid steel diminishes asymptotically from its highest value at the wall of the orifice in moving toward the axis. Also, the electromagnetic force near the wall of the **throat** of the orifice is much stronger than that in the entrance or exit regions of the ESZ.

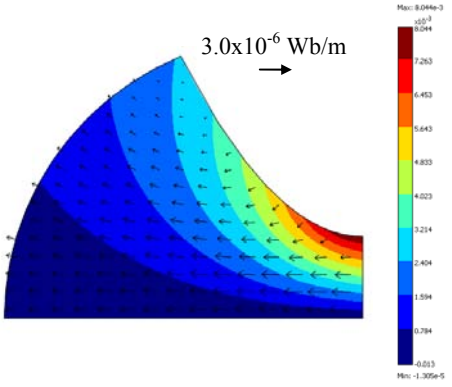

Fig 1: Self-induced magnetic field distribution ***B***, within the ESZ for a DC current I=15A, and 500 μm diameter orifice. The magnetic vector potential ***A*** indicates by arrows, the colour contours stand for the magnetic flux density, ***B*** (max. ~8mT).

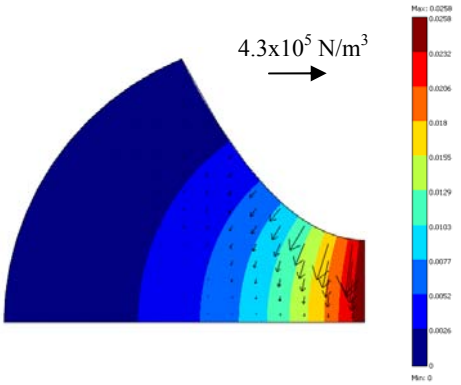

Fig 2: The electromagnetic force distribution. Color contours represent the electric potential ***E*** and the arrows note the vectors of the electromagnetic force.

4.2 Fluid field:

The predicted flow field for a 500 μm (the diameter at the throat) orifice with an initial normal velocity of 0.15m/s is shown in Fig 3. The flow field with moderate (Fig 3a, I=15A) and much higher (Fig 3b, I=300A) input current are investigated. In the former case, the axial velocity is very uniform at each section along the ESZ except near the boundary layer adjacent to the wall of the ESZ. This is the case for normal operating conditions for the detection of inclusions within the liquid steel. In the latter case, the much higher magnetic pressure near the wall of the orifice pushes back downstream as a huge flow obstacle. As a consequence, a reverse flow is generated, and the maximum velocity then increases significantly. According to the principle of LiMCA, this situation should be avoided during normal operations in order to allow entrained inclusions to pass through the ESZ successfully. However, our research with aluminum melts has shown that such over-imposing currents can effectively remove any inclusions accumulating on the walls of the orifice. Indeed, to ensure that the orifice is clean at the start of an inclusion sampling measurement, a heavy current is purposefully used for aluminum melts (not steel), to scour out any accumulating 'rafts' of inclusions at the entrance to the ESZ.

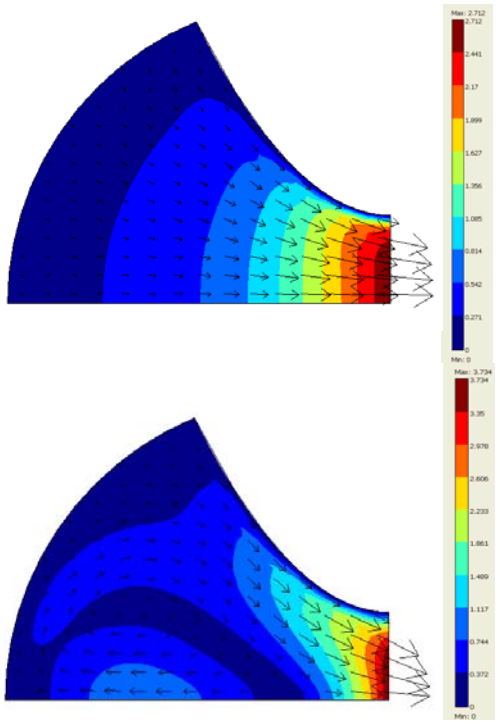

(b)

Fig 3: Flow fields and flow patterns.
(a) I=15A; (b) I=300A.

4.3 Inclusion trajectories:

Once the fluid flow and the electromagnetic fields within the ESZ are known, Eqs(6-7) can be solved to predict the motion of inclusions.

Note that according to the LiMCA principle, the residence time of the inclusion passing through the ESZ is very important. It is in the order of milliseconds. In practise, the number density of inclusions is sufficiently low that only single inclusions are entrained in the ESZ at any one time. The predicted trajectories of twelve Al_2O_3 ($\rho_p = 3800 kg/m^3$) inclusions are shown in Fig 4 only for convenient comparison of the effect of initial locations. In the Comsol software, these predicted particle trajectories do not disturb each other at all.

The size of the inclusions chosen was 100μm. As seen in Fig 4a, at I=15A, the inclusions successfully pass through the ESZ, the trajectories following the flow stream indicates that the inertial force play the dominant role in determining their hydrodynamics. Also, in the entrance region, the particle moves very slowly, but then accelerates rapidly to its highest value near the throat of the orifice. However, at 300 Amps, the magnetically induced back pressure generates a recirculating flow, as shown in Fig 4b. In this case, incoming inclusions flow towards the side walls of the ESZ, and possibly attach and sinter. These trajectories are mainly influenced by the fact that non-conducting inclusions experience an electro-magnetic force that is in the opposite direction to those acting on the liquid steel (Fig.2). These forces are wall-directed, since buoyancy forces are negligible. As a consequence, the recirculating flow exacerbates and accelerates the motion of any inclusions towards the sidewall of the ESZ.

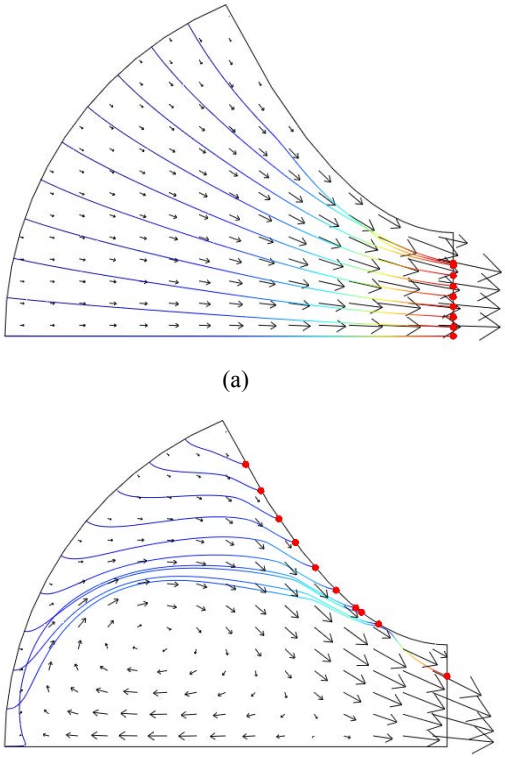

(a)

(b)

Fig 4: Predicted trajectories of inclusions (d=100μm) and steel flow vectors, when passing DC currents of (a) I=15A.and (b) I=300A, through liquid steel passing through a 500 micron (throat) diameter ESZ.

4.4 Discrimination of inclusions based on transient electric resistance pulses

When an inclusion passes through the ESZ, a transient voltage (or resistance) pulse will be formed. Seven parameters: peak height, peak time, peak width, start and end slope, start and end time are used to characterize the pulse [3]. With the help of Eq.(12), predicted resistive pulse for three sizes of inclusion: 50μm, 100μm and 150μm as function of z-axis is shown in Fig 5. As seen, the voltage pulse distribution is very like a normal Gaussian curve. Obviously, the larger the size of inclusion, the higher is the peak height of pulse registered. The peak height of 150μm is about seventeen times that of a 50μm particle.

It is necessary to note that the original entry points of the inclusions for these predictions are located on the asymmetrical axis in Fig 5. More generally, this mathematical model allows us to predict the pulses that would be generated by an inclusion originating from any initial entry point.

In practice, we measure time-dependent transient pulse signals, not space-dependent ones, so we need to transform from the latter to the former. This Comsol numerical model can accomplish this task: since we know the transit time at each position along an inclusion's trajectory; we can then predict how the transient pulse varies as the motion of the inclusion evolves with time. The transit time is about 3 milliseconds for an inclusion size d=100μm, but the change in the electric resistance indicates a smaller value of about 2 milliseconds. This is caused by the much lower flow velocity in the entrance region, and the small magnitude of the resistance change in that region.

As mentioned in the introduction, a laboratory scale water-based LiMCA system was developed to accompany the development of the metal-based LiMCA system. The main difference between them lies in the physical properties of the fluid in terms of electrical conductivities, viscosities and densities. Despite these, they perform equivalently, minus the induced electromagnetic forces on the inclusions in aqueous systems, where currents are only ~ 20 mA.

Figs6(b, c) shows a typical measurement signal generated by a silica particle in the water based LiMCA system [8, 9], in which they yield similarly shaped start and end slopes to those predicted in Fig 6(a). The transit time of the inclusion in the water LiMCA system was set ten times lower in those experiments. In both cases the peak height represents the inclusion passing the throat of the orifice. This information, in turn, with the help of Eq.(11-12), allows us to determine the mean diameter of each inclusion. With this, we can discriminate on the basis of size, and provide information on the size distribution. It is also possible to discriminate on the basis of inclusion density, but this goes beyond the topics addressed in this paper.

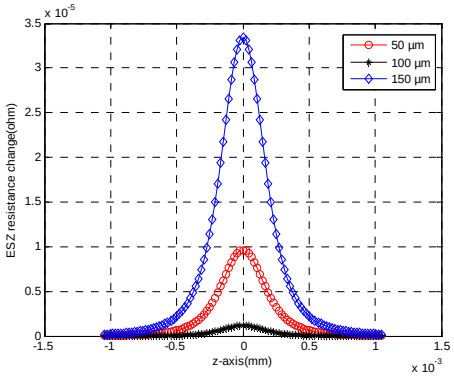

Fig 5: ESZ resistance change with the position of non-conductive particles of various diameters.

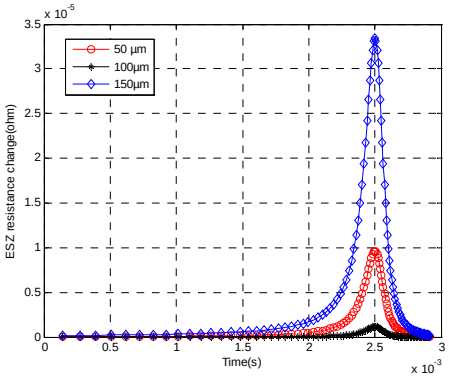

Fig 6a: Numerically predicted transient electric pulse vs. residence time of an inclusion (d=100 μm) passing through the ESZ.

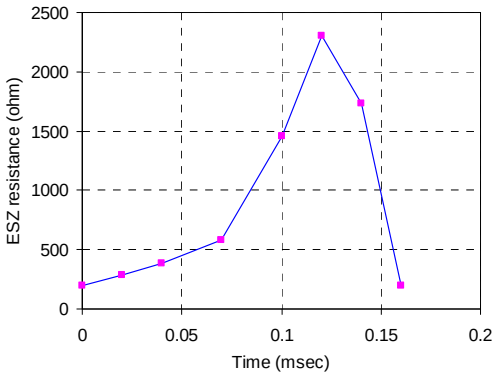

Fig 6b: Typical ESZ resistance signal generated by a silica inclusion (d=150 µm) using the APS II unit (250 mmHg pressure drop across the LiMCA probe) [8].

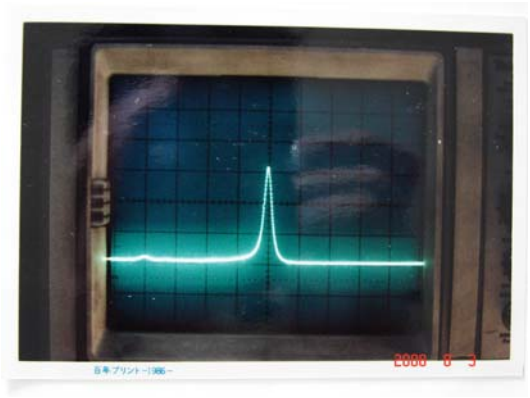

Fig 6c: Voltage pulse detected by oscilloscope during passage of a silica particle (diameter d=100µm), through a rounded orifice with throat diameter D=500 µm), aspiration speed 8 m/s [9].

5. Conclusions

A mathematical model is proposed using the Comsol software package to predict the behavior of inclusions in a liquid steel LiMCA system. The equation-based solutions provide us information on the influence of the drag, the added mass, inertial effects, and most significantly, electromagnetic forces, on the motions of the inclusions. It can predict the fate of inclusions entering the ESZ, compute transient electric resistances, and provide insights into the experimental resistive pulses recorded in practice.

Additionally, this Comsol model allows for parametric studies of inclusions physical properties such as the role of their electric conductivities, their relative densities, different sizes, or other physical characteristics (solid inclusions, micro-bubbles, or micro-droplets). Similarly, different kinds of liquid metals can be simulated, such as aluminum, copper, zinc as well as liquid steel. Finally, the present numerical predictions are being compared with industrial data obtained using LiMCA equipment in the non-ferrous, light metal, and steel industries.

6. References

1. D. Doutre, R.I.L.Guthrie, U.S. Patent 4,555, 662 (1985)
2. R.I.L.Guthrie, D. Doutre, Proc. Int. Seminar on Refining and alloying of liquid aluminum and Ferro-alloys, Trondheim, Norway, pp.146-163. (1986)
3. R.I.L.Guthrie, M. Li, In situ diction of inclusions in liquid metals: Part I: Mathematical modeling of the behavior of particles traveling the electric sensing zone, *Metallurgical and materials transaction B*, **Vol.32B**, pp.1067-1079 (2000)
4. M. Li, R.I.L.Guthrie, Numerical studies of the motion of particles in current-carrying liquid metal flowing in a circular pipe *Metallurgical and materials transaction B*, **Vol.31B**, pp.357-363 (2000)
5. A. M. Fayon, J. Happel, Effect of a cylindrical boundary on a fixed rigid sphere in a moving viscous fluid, *AIChE*, **Vol.6**, pp.55 (1960)
6. J. Happel and H. Brenner, Low Reynolds number hydrodynamics, Printice-Hall, Inc., Englewood Cliffs, N.J., pp.331 (1965)
7. J.C. Maxwell, A Treatise on electricity and magnetism, 3rd Ed., Clarendon, Oxford. **Vol.1**, pp.429 (1954)
8. C. Carozza, Water modelling of particle discrimination using LiMCA technology, *master thesis*, McGill University, pp.57 (1999)
9. S. Tanaka, Modelling inclusion behaviour and slag entrainment in liquid steel processing vessels, Ph.D. *thesis*, McGill University, pp.70 (1986)